Slow, heterogeneous NFκB single molecule conformational dynamics and implications for function

Wei Chen1, Wei Lu[2], Peter G. Wolynes[2] and Elizabeth A. Komives[1],*

[1]Department of Chemistry and Biochemistry, University of California, San Diego, 9500 Gilman Drive, La Jolla, CA 92093-0378.

[2] Center for Theoretical Biological Physics, Departments of Chemistry, Physics, and Biosciences, Rice University, Houston, Texas, United States of America.

*Elizabeth A. Komives
Email: *ekomives@ucsd.edu

Abstract

Single-molecule FRET was used to probe the interdomain motions of the transcription factor NFκB. A continuum of conformations interconverting on hundreds of milliseconds to minutes were directly visualized. The widely different timescales of the motions suggest a hierarchical rugged energy landscape. Even when bound to DNA, the domains remain mobile with the conformational distribution shifted to two major populations; a high-FRET state expected from the NFκB-DNA x-ray structure and a low-FRET state consistent with one of the DNA-binding domains dissociated. When bound to the inhibitory protein IκBα, which is known to accelerate DNA dissociation and block DNA binding, the interdomain motions were locked into a low-FRET state. Binding to the IκBα mutant unable to accelerate DNA dissociation failed to lock the interdomain motions. Our results suggest that the slow, heterogeneous motions of NFκB are essential in regulating the kinetics of DNA association and dissociation to achieve efficient transcription activation and termination.

Introduction

Internal motions of proteins are important for their functions. Such motions are crucial for cell signaling and regulation, where a precise control is needed for turning on and off an event [1]. These regulations are achieved through a series of protein-protein and protein-nucleic acid interactions accompanied by conformational changes. In these association and dissociation reactions, protein motions can affect binding rates/affinities and respond to allosteric regulators, therefore ultimately controlling the timing and precision of a cellular event.

Motions of a protein arise as a result of its navigation through the energy landscape. Although often being associated with folding funnels [2], the concept of energy landscape emerged from early photodissociation experiments, in which nonexponential kinetics suggest multiple conformations instead of a single structure for myoglobin at low temperature [3,4]. Recent single-molecule experiments and simulations on enzymes further suggest multiple near-continuous conformations and subdiffusive dynamics on a rugged energy landscape by showing a power-law distribution of dwell times in observed states [5-7].

Here, we describe direct visualization of a continuum of conformations and the motions connecting them for the transcription factor NFκB with single-molecule FRET (smFRET). Here, NFκB is a heterodimer formed by the subunits RelA and p50, although dimerization of other NFκB family members occurs and is prevalent in eukaryotic transcription factor families [8]. Theoretical studies suggest that the relative motions of the two DNA-binding domains in a transcription factor dimer could control the search and recognition of target DNA [9]. However, experimental characterization of such motions is challenging because they cannot be understood with static pictures or studies on individual domains. It remains largely unknown how the domains are oriented with respect to one another in protein assemblies, how they re-orient during macromolecular interactions, and how the interdomain motions affect molecular recognition.

The NFκB monomer in this study, RelA or p50, each consists of a dimerization domain (DD) and a N-terminal DNA-binding domain (NTD) connected by a 10-amino acid linker. The NFκB heterodimer recognizes the consensus κB DNA sequence with its two NTDs (Fig. 1A). No crystal structures are available for NFκB in the absence of binding partners. We previously showed using molecular dynamics (MD) simulations corroborated by hydrogen-deuterium exchange experiments that the flexible linkers allow the two NTDs to undergo large-scale interdomain motions which leads to exposure of the DNA-binding cavity[10].

In the absence of stimuli, NFκB is held inactive in the cytoplasm by the inhibitor protein, IκBα. Upon stimulation, NFκB-bound IκBα is phosphorylated, ubiquitylated, and then degraded (Fig. 1C) [11], allowing the exposure of the NFκB nuclear localization signal and the translocation of NFκB from the cytoplasm to the nucleus. NFκB activates the expression of hundreds of genes, including the one of its own inhibitor, IκBα.This creates a negative feedback loop in which the newly synthesized IκBα enters the nucleus, binds to NFκB to block DNA binding [12], and return the NFκB-IκBα complex to the cytoplasm [13].

As a master regulator of a large number of genes, the termination of NFκB signaling is efficient. Previous kinetic experiments revealed molecular stripping—a process in which IκBα actively removes NFκB from DNA [11]. This discovery suggests that the termination of NFκB signaling is not just an equilibrium result of IκB outcompeting DNA for binding but rather it is achieved kinetically through IκBα-accelerated dissociation of NFκB from DNA. A transient ternary complex was observed during molecular stripping, and the DNA dissociation rate is proportional to the IκBα concentration [14]. A stripping impaired IκBα mutant generated by neutralizing the negatively PEST sequence (5xPEST) results in slower nuclear export of NFκB in the cell indicating that the stripping rate controls the nuclear export rate[15]. Although the relative orientation of the NTDs in NFκB-IκBα is unknown from crystal structures due to domain truncations (Fig. 1B) [16,17], coarse-grained MD simulations suggest that the NTD motions and

their responses to IκBα binding play a key role in molecular stripping by lowering the DNA dissociation barrier [18,19].

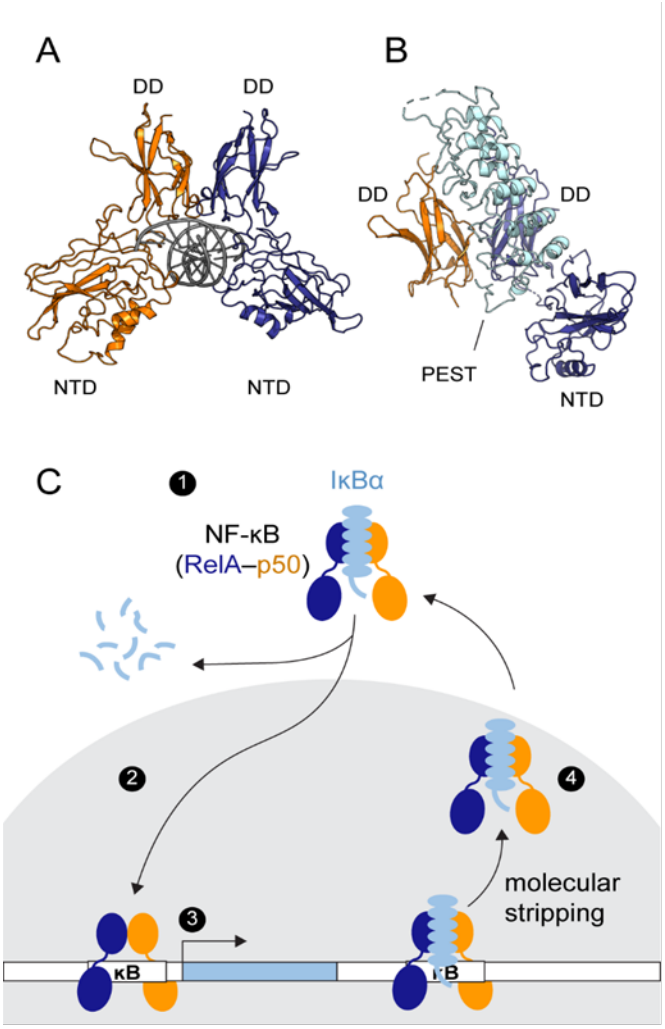

Fig. 1. Transcriptional regulation by NFκB (*A*) Structure of the NFκB RelA-p50 heterodimer bound to DNA (PDB: 1LE5, RelA in blue, p50 in orange, and DNA in grey). Each NFκB monomer contains a dimerization domain (DD) and a N-terminal DNA binding domain (NTD) connected by a 10-amino-acid linker. The NFκB dimer recognizes its cognate DNA through the two NTDs (*B*) Structure of the NFκB-IκBα complex (PDB: 1IKN, IκBα in cyan). IκBα binds to the DDs of NFκB. The disordered PEST sequence is at the C-terminus of IκBα. The NTD of p50 was truncated in order to achieve crystallization. (*C*) Schematic of NFκB transcriptional regulation showing 1) NFκB held in the cytoplasm bound to IκBα. 2) Upon signal input, IκBα is degraded freeing NFκB to enter the nucleus (grey). 3) NFκB binds to DNA and turns on hundreds of genes, one of which is that for IκBα, creating newly synthesized IκBα. 4) IκBα enters the nucleus and strips NFκB from the DNA returning it to the resting state.

Here we report the interdomain motions of NFκB in the free, DNA-bound, and IκBα-bound states revealed by TIRF-based smFRET. By labeling the two NTDs with a FRET pair, we directly visualized the time trace of interdomain distance fluctuation for each single NFκB dimer. Remarkably, a continuum of interdomain distance from 30 Å to 70 Å were found with motions on the hundreds of milliseconds to minutes timescale. The NTDs remained mobile even when bound to DNA, but in this case the conformational ensemble was shifted. Binding of IκBα appears to completely lock the NFκB NTDs into a single conformation consistent with NTDs being spread apart, while binding of stripping-impaired 5xPEST IκBα failed to lock the motions. We speculate that despite the fact that such slow and heterogeneous motions have not, to our knowledge, been reported in other protein systems, they are essential for efficient molecular stripping and readily account for the intracellular kinetics observed for NFκB.

Methods

Protein expression, purification, and labeling. Plasmids of murine RelA1-325 (UniProt entry Q04207) and p5039-363 (UniProt entry P25799) in pET11a vectors (Plasmid #44744, Addgene) were provided by Gourisankar Ghosh at UCSD. A 6xHis-tag was introduced to the C-terminus of RelA by site-directed mutagenesis for immobilization. Q128 of RelA and F148 of

p50 were mutated into Amber stop codons TAG by site-directed mutagenesis for unnatural amino acid incorporation and fluorophore labeling. Plasmid containing RelA or p50 was co-transformed with pEVOL-pAzF (Plasmid #31186, Addgene), the plasmid encoding the aaRS/tRNA pair for incorporating the unnatural amino acid p-azidophenylalanine (pAzF, CAS 33173-53-4, Chem-Impex Int'l. Inc.), into BL21 (DE3) E. coli strain (New England Biolabs). Cells were first grown in M9 minimal media with 200 mg/L ampicillin and 34 mg/L chloramphenicol at 37 °C and 180 rpm. At 0.6 - 0.7 OD600, the expression of RelA or p50 was induced with 0.2 mM IPTG, and the expression of the aaRS/tRNA was induced with 0.02% L-arabinose. pAzF was added to a 200 mg/L final concentration. Cells were then grown at 18 °C and 180 rpm for 16 hours and harvested by centrifugation at 5,000 rcf for 15 minutes. The cell pellet containing His-tagged RelA was resuspended in 50 mM sodium phosphate pH 8, 150 mM NaCl, 10 mM imidazole, 0.5 mM PMSF with protease inhibitor cocktail (Sigma-Aldrich). Following sonication on ice, the cell lysate was centrifuged at 17,000 rcf for 30 minutes. The supernatant was passed through Ni-NTA resins (Thermo Fisher Scientific) and washed with 10 column volumes of the wash buffer (50 mM sodium phosphate pH 8, 150 mM NaCl, 20 mM imidazole). RelA was eluted with 50 mM sodium phosphate, 150 mM NaCl, 250 mM imidazole. Elution was pass through a PD 10 desalting column (GE Healthcare) to remove imidazole and eluted with 25 mM Tris pH 7.5, 150 mM NaCl, 0.5 mM EDTA. After added the protease inhibitor cocktail and glycerol (5% final concentration), the sample was aliquoted and stored at -80 °C for further fluorophore labeling and purification. The cell pellet containing non-tagged RelA or p50 was resuspended in 25 mM Tris pH 7.5, 150 mM NaCl, 0.5 mM EDTA, 0.5 mM PMSF. After sonication and centrifugation, the supernatant was passed through SP Sepharose Fast Flow resins (GE Healthcare). An NaCl gradient from 0 to 700 mM NaCl was used to elute the protein. The elution fraction was purified with a PD10 desalting column and stored in 20 mM Tris pH7.5, 150 mM NaCl, 0.5 mM EDTA, 5% glycerol at -80 °C. Reducing agents was avoided to prevent reducing pAzF to pAmF (p-aminophenylalanine). Expression of full-length RelA1-325 and p5039-363 was confirmed by SDS-PAGE. Site-specific incorporation of pAzF was further confirmed by pepsin digestion and tandem mass spectrometry. Peptides DLE*AISQR (M+H 1093.567, residues 126 – 133 of RelA) and GILHVTKKKV*ETL (M+H 1653.984, residues 138 – 161 of p50) containing pAzF (denoted by asterisk) were identified. Fluorophore labeling was achieved through the copper-free click reaction between the azido sidechain of the incorporated pAzF and the sDIBO functional group on the fluorophore. RelA and p50 were thawed from -80 °C and labeled separately with Click-iT™ Alexa Fluor™ 555 sDIBO Alkyne (FRET donor, Thermo Fisher Scientific) or Click-iT™ Alexa Fluor™ 647 sDIBO Alkyne (FRET acceptor, Thermo Fisher Scientific) with a 1:2 protein-to-dye molar ratio at 4 °C for 2-7 days. The FRET radius R0 of the donor/acceptor pair used in this study is 51 Å. Excess dyes were removed with PD10 desalting columns. Labeling efficiency was determined with the extinction coefficients (εRelA280 = 20,400 M-1 cm-1, εp50280 = 23,380 M-1cm-1, εAlexa555555 = 155,000 M-1cm-1, εAlexa647650 = 239,000 M-1cm-1) and the correction factors accounting for A280 from the dyes (CFAlexa555 = 0.08, CFAlexa657 = 0.03). The labeling efficiency is 29% to 56 % for Alexa Fluor 555 to RelA, 20% to 35% for Alexa Fluor 647 to RelA, 52% to 83% for Alexa Fluor 647 to p50, and 18% to 50% for Alexa Fluor 647 to p50. Labeled RelA and p50 were mixed with a 1:5 donor:acceptor molar ratio to form RelA-p50 heterodimer. The dual-labeled heterodimer was then purified by cation exchange chromatography (Mono S 10/100, GE Healthcare) in 25 mM Tris pH 7.5, 0.5 mM EDTA, 1mM DTT with an NaCl gradient from 100 to 700 mM and size exclusion chromatography (Superdex 200, GE Healthcare) in Tris pH 7.5, 150 mM NaCl, 0.5 mM EDTA, 1mM DTT as previously used for wildtype RelA-p50 heterodimer [20].

Human IκBα67-287 (Uniprot entry P25963) in pET11a was introduced with a N-terminal 6xHis tag. The 5xPEST IκBα had the following mutations: E282Q/E284Q/D285N/E286Q/E287Q and was expressed and harvested as previously described for nontagged IκBα [21]. Cell lysates were passed through Ni-NTA resin equilibrated in buffer A (25 mM Tris pH 7.5, 150 mM NaCl,

10 mM imidazole, 10 mM βME), washed with wash buffer (25 mM Tris pH 7.5, 150 mM NaCl, 20 mM imidazole, 10 mM βME), and eluted with buffer B (25 mM Tris pH 7.5, 150 mM NaCl, 250 mM imizadole, 10 mM βME). Fractions containing IκBα were then dialyzed overnight at 4°C in SEC buffer containing 25 mM Tris pH 7.5, 150 mM NaCl, 0.5 mM EDTA, 1mM DTT. The dialyzed protein was then either frozen in 2 mL aliquots at −80°C until needed or immediately further purified from aggregates by size exclusion chromatography (Superdex S75; GE Healthcare) in SEC buffer. The IκBα concentration was determined with the extinction coefficient εIκBα280 = 12,950 M-1 cm-1

Single-molecule FRET data collection. A prism-type total internal reflection fluorescence (TIRF) microscopy was used. For Alexa Flour 555/ Alexa Flour 647 dye pair, a 532 nm laser (SAPPHIRE 532-300 CW CDRH, Coherent) and a 637 nm laser (OBIS™ 1196625 | 637nm LX 140mW Laser, Coherent) were set up to excite donor and acceptor respectively. Laser output powers were set to 50 mW for smFRET experiments. 532 nm and 637 nm laser beams were guided by mirrors and a beam splitter to colocalize on the excitation area on the prism. An inverted microscope was set up by mounting the objective (CFI Plan Apochromat VC 60XC WI, Nikon) on a Rapid Automated Modular Microscope System (Applied Scientific Instrumentation). Emission light was further split into donor and acceptor channels with a DV2 Two-Channel, Simultaneous-Imaging System (Photometrics) with band pass filters (ET585/65m for donor channel and ET685/56m for acceptor channel, Chroma). Fluorescent signals were detected by Electron Multiplying Charge-Coupled Device (EMCCD) (iXonEM+ EMCCD camera, DU-897E-CS0-#BV, Andor Technology). DDS-Tween 20 passivated surface [22] with 0.2 mg/mL biotinylated bovine serum albumin (A8549, Sigma-Aldrich) and 0.2 mg/mL NeutrAvidin (31000, Thermo Fisher Scientific) were used to immobilize NFκB. For free NFκB experiments, NFκB molecules were immobilized through the 6xHis-tag on the C-terminus of RelA by penta-His antibody biotin conjugate (34440, Qiagen). For DNA-bound NFκB experiments, DNA-NFκB complexes were immobilized through the biotinylated hairpin DNA containing the underlined κB sequence:

Biotin-GCATGCGGGAAATTCCATGCATGCCCCCCATGCATGGAATTTCCCGCATGC

For IκBα-bound NFκB experiments, IκBα-NFκB complexes were immobilized through the 6xHis-tag on the N-terminus of IκBα.

Experiments were performed at room temperature in imaging buffer (25 mM Tris pH 7.5, 150 mM NaCl, 0.5 mM EDTA, 0.8 mg/mL glucose oxidase (G2133, Sigma-Aldrich), 0.2 mg/mL catalase (219001, CALBIOCHEM), 0.4% dextrose, and 5 mM Trolox (CAS 53188-07-1, Sigma-Aldrich)). Trolox was prepare by dissolving 10 mg Trolox powder in 10 mL of 25 mM Tris, pH 7.5, 150 mM NaCl, 0.5 mM EDTA with vortexing for 30 minutes and then incubation at room temperature and ambient light overnight. The 637 nm laser was used to confirm the existence of acceptor fluorophores and the 532 nm laser was used for excitation of the donor fluorophore. Data acquisition and analysis software was obtained from the Ha Lab at Johns Hopkins University http://ha.med.jhmi.edu/resources/#1464200861600-0fad9996-bfd4. Single molecule movies were recorded with 100 ms time resolution.

Single-molecule FRET data analysis. Individual single-molecule traces were extracted from the acquired movies with the IDL scripts in the Ha Lab software package. The traces were further selected based on the criteria: (i) clear single photobleaching step for both donor and acceptor; (ii) anticorrelation pattern for donor and acceptor intensities; (iii) stable total fluorescence intensity before photobleaching; (iii) > 10 sec photobleaching lifetime for both donor and acceptor. Time periods with no signals caused by donor or acceptor dark states, an unbound state, or a state in which an unlabeled NFκB is bound to the immobilized DNA or IκBα were excluded. For each trace, background was defined as the mean values of the donor and acceptor fluorescence intensities after photobleaching and subtracted from the data. To account for the donor signal leakage to the acceptor channel, we measured the correction factor by collecting data of Alexa Flour 555 labeled RelA. After background subtraction for individual

traces of Alexa Flour 555 labeled RelA, the correction factor was defined as the mean value of the ratio of the acceptor intensity to the donor intensity and calculated to be 0.04. Therefore, for a single-molecule trace, the background and donor leakage are corrected by the following equation in which I is the fluorescent intensity:

$$I_{donor} = I_{donor}^{raw} - I_{donor}^{background}$$

$$I_{acceptor} = I_{acceptor}^{raw} - I_{acceptor}^{background} - 0.04 \times I_{donor}$$

The FRET efficiency (E) was calculated using the corrected fluorescent intensities. E = Iacceptor / (Idonor + Iacceptor). Finally, traces were categorized as fluctuating based on whether the signal fluctuations were larger than that caused by noise (shown in the signal after photobleaching). Traces with no fluctuations larger than noise were categorized as stable.

FRET data were presented in two types of histograms. In the first type, the first 1000 timepoints (10 seconds) of each trace were used as data points to build the histogram. In the second type, fluctuating traces were not included, and mean FRET efficiency values of each individual long-lived state were used as data points to build the histogram. The first type of histogram built by counting timepoints is useful for general purposes and the second type built by counting visits to long-live states eliminated noise and was used to show the continuous distribution of states.

Fluctuating traces were subjected to cross-correlation analysis. The cross-correlation function is defined as previously described [23]. Only traces longer than 30 seconds were included in the analysis and the correlation up 15 seconds were calculated. Results were fitted with a bi-exponential function to compare the characteristic fluctuation time.

Molecular simulations and analysis. We used OpenAWSEM [24] to model the heterodimer-DNA complex. The initial structures of the protein and DNA were from the crystal structure of NFkB (PDB entry: 1LE5). We extended the DNA sequence 100 pairs of A/T at both ends to reduce any finite size effect caused by having a short DNA sequence. The protein and DNA were initially placed far away from each other. Chain A (RelA) of the protein was shifted 300 Å to the left along the x axis from the DNA and chain B (p50) was shifted 300Å to the right. As the simulation began, both chains of the protein were pulled toward the DNA with a native protein-DNA contact bias. This bias was turned off after 10 million steps. Then, we ran another 10 million steps of unbiased simulation. We used a Langevin integrator with a friction of 1 ps-1 and a step size of 2 fs. The simulations were carried out at constant temperature of 300 K. The default strength for each term followed our previous study [19], with Vcontact=0.75, VHB=0.5. We did not use a Gō term in this study. The fragment memory consisted of nine equally weighted structures. Among them, one was the crystal structure, and the other 8 structures are sampled from two independent all-atom simulations [10] at 100, 200, 300, and 400 ns. The simulations were repeated 20 times with the same initial structures but different initial velocities and different random seeds. The trajectories were saved every 4000 steps and the last 2000 frames were used for analysis.

Results

Conformational Heterogeneity in Free NFκB. Previous coarse-grained [18] and all-atom MD simulations [10] showed that the two NTDs in a NFκB dimer can rotate and translate with respect to each other. To experimentally probe the conformational heterogeneity of the NTDs, we carried out TIRF-based smFRET experiments by labeling each NTD with either a donor or acceptor fluorophore. We replaced RelA Glu128 and p50 Phe148 with p-azidophenylalanine (pAzF) by amber suppression and then labeled these two residues specifically with either Alexa Fluor 555 or Alexa Fluor 647 sDIBO alkyne via click chemistry [25,26]. The distances between the labeling positions in the NFκB-DNA crystal structure [27] and in an open conformation obtained from previous all-atom simulations [10] are 27 Å and 70 Å respectively, which correspond to 0.1 and 1 in FRET efficiency given the dye pair R0 of 51 Å (Fig. 2A).

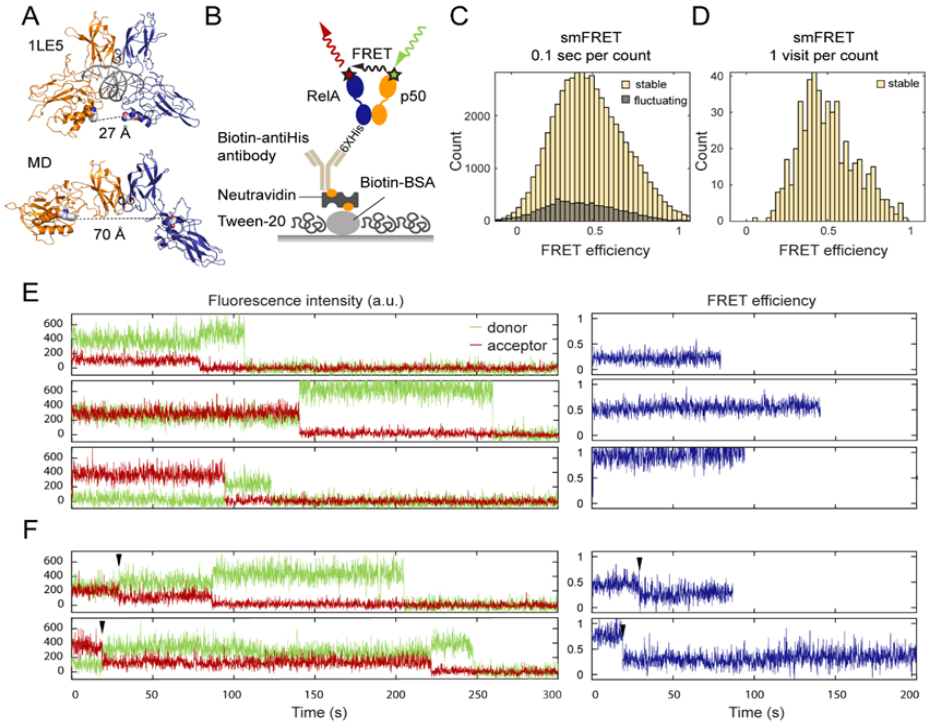

Fig. 2. smFRET experimental design for probing the relative domain motions of NFκB. (*A*) In the NFκB-DNA crystal structure (PDB: 1LE5), the distance between the two labeled positions; E128 in RelA and F148 in p50 (spheres), would lead to a high FRET efficiency ~1. In MD simulations, free NFκB could adopt an open conformation, leading to a low FRET efficiency ~0.1. (*B*) Schematic of how the NFκB was immobilized on a DT20 passivated surface via the His-tag on RelA, biotin-conjugated anti-His antibody, NeutrAvidin, and biotin-conjugated bovine serum albumin (BSA). The two NTDs were labeled with FRET donor (green star) and acceptor (red star). (*C*) FRET histogram showed a broad distribution of conformations. The histogram was constructed by counting the first 10 seconds of the traces. (*D*) FRET histogram constructed by counting each visit to a long-lived state suggested a continuous distribution of stable states that cannot be separated into a few groups. (*E*) Representative stable smFRET traces with low, mid, and high FRET efficiencies. Other long-lived states with different FRET efficiencies are shown in SI. (*F*) Transitions (arrowhead) between long-lived states were captured.

The dual-labeled NFκB was immobilized on the DT20 passivated slide [22] through a series of interactions between the C-terminal His-tag on RelA, biotin anti-His antibody, NeutrAvidin, and biotin-bovine serum albumin (BSA) (Fig. 2B). We collected 426 smFRET traces for free NFκB (Fig. S6-32). Each smFRET trace covers between 10 and 300 seconds depending on the photobleaching lifetime of the fluorophores. The experimental FRET histogram, calculated from the first 10 seconds to avoid bias caused by long traces, showed a broad distribution in FRET efficiency from 0.1 to 1 (Fig. 2C), revealing a conformational heterogeneity which corresponds to approximate distances of 30 Å to 70 Å. The distances we report are close estimates based on rigorous background and donor leakage corrections. Obtaining accurate distances from smFRET requires alternating two-color laser excitation [28] and is not the focus of this work.

Heterogeneous Long-Lived States in Free NFκB. The smFRET traces were further classified as stable (82% of the traces) or fluctuating (18% of the traces) (Fig. 2C, S6-32). A stable trace was defined as containing long-lived state(s) with lifetimes longer than the photobleaching lifetime in that trace, which averages 90 sec (Fig. S1). In most stable traces, the single NFκB molecules spent the entire observation time in one long-lived state until photobleaching. In long-lived states, there is no anticorrelation between donor and acceptor signals (Fig.S2). A broad range of long-lived states with low- to mid- to high-FRET efficiencies were all observed (Fig. 2E, S6-32). Occasionally, there were transitions between two states in a trace (Fig. 2F), indicating these long-lived states are interconvertible via slow dynamics likely in the minutes timescale. To avoid broadening in the histogram caused by noise, a histogram for long-lived states was built by binning the mean FRET efficiency of each visit to a long-lived state (Fig. 2D). The histogram constructed in this way showed that these long-lived states could not be separated into a few groups amenable to hidden Markov modeling. Instead, we observed a

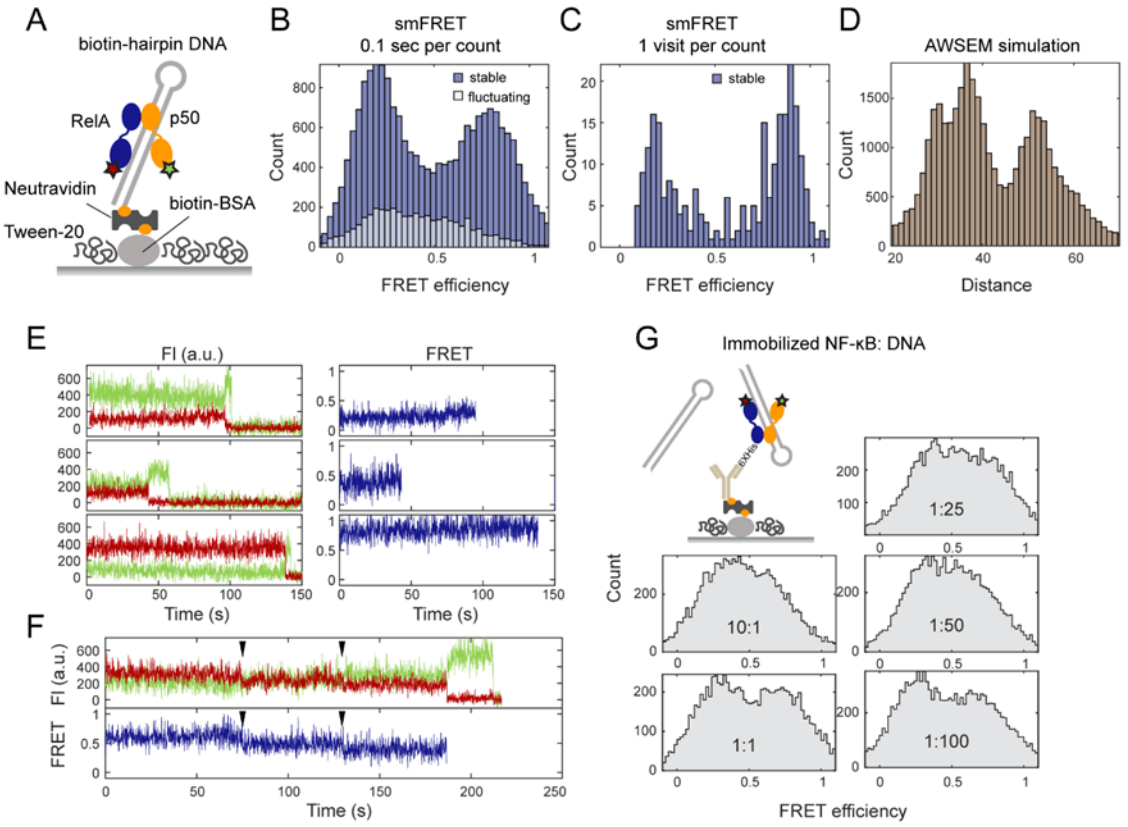

Fig. 3. smFRET experiments for DNA-bound NFκB. (A) Schematic of the experimental set-up. A biotinylated hairpin DNA with a κB site was used for immobilization through biotin-NreutrAvidin interactions. (B) FRET histogram showing two major populations at low and high FRET efficiencies contributed by stable traces. (C) FRET histogram constructed by counting each visit to a long-lived state showing a continuous distribution with two dominating populations. (D) Distribution of the distance between labeling positions sampled with AWSEM simulations showing two dominating populations in DNA-NFκB. (E) Representative stable traces showing long-lived states with low, mid, and high FRET efficiencies. (F) A representative trace showing transitions between long-lived states from high to mid to low FRET efficiencies. Other long-lived states with different FRET efficiencies are shown in SI (G) smFRET titration experiments with immobilized NFκB and varying DNA concentrations. A series of NFκB:DNA molar ratios from 10:1 to 1:100 showed similar FRET histograms with a broad band from free NFκB and two slightly higher peaks at low and high FRET efficiencies.

heterogeneous, continuous distribution. A continuum of long-lived states and transitions between them were still observed in the presence of DTT, indicating that the heterogeneity was not caused by formation of disulfide bonds (Fig. S3).

DNA binding shifts the distribution of Long-Lived States. To investigate how DNA-binding affects the relative positions and the motions of the two NTDs, we carried out smFRET experiments with NFκB bound to a biotinylated hairpin DNA containing the IFN κB binding site which was immobilized on the passivated surface through biotin-NeutrAvidin interactions (Fig. 3A). By immobilizing through biotinylated DNA, we ensured that every NFκB molecule we observed is DNA-bound. We collected 199 smFRET traces for DNA-bound NFκB, of which 84% could be categorized as stable—containing long-lived state(s) with lifetimes longer than the photobleaching lifetime. (Fig. S1, S33-43). Surprisingly, DNA did not shift the conformational ensemble to a single high-FRET state as expected from the crystal structure (Fig. 2A), but instead shifted the distribution of long-lived states to a distribution of populations which included a high-FRET population in good agreement with the crystal structure as well as an unexpected low-FRET population (Fig. 3B,C). Traces in which molecules sampled a distribution of mid-FRET states were also observed (Fig. 3E, S33-43). As was the case for free NFκB, transitions between long-lived states were captured, indicating motions likely on the minutes timescale (Fig. 3F).

Since all crystal structures of DNA-bound NFκB indicate a ~30 Å distance between the labeling positions (PDB entries: 1VKX, 1LE5, 1LE9, 1LEI, 2I9T, 2O61, and 3GUT), it is surprising to observe a major population at low FRET efficiency. A crystal structure of NFκB p50 homodimer bound to two double-stranded RNA molecules [29] suggested that the observed low FRET state could be caused by binding to two DNA molecules on the surface of the microscope slide. To test this possibility, we carried out smFRET titration experiments, this time immobilizing the NFκB and adding a range of DNA concentrations (Fig. 3G). If the low-FRET state was a conformation caused by binding to two DNA molecules, the relative peak height for the low-FRET population would be expected to increase with the DNA concentration. It is important to note that because the NFκB is immobilized, we expect a population of free NFκB to contribute to the histogram. The results showed that a range of NFκB:DNA molar ratios from 10:1 to 1:100 lead to almost identical FRET histograms built by counting the first 10 seconds. Each histogram appears to have two slightly higher peaks at high and low FRET efficiencies contributed by DNA-bound NFκB superimposed on the broad distribution expected from free NFkB (Fig. 3G). The independence of the FRET histogram on the DNA concentration suggests that the low-FRET state was not a conformation resulting from binding to two copies of DNA but is likely a conformation with one NTD dissociated from DNA.

We turned to coarse-grained AWSEM simulations [18,24] to understand whether NFκB bound to one copy of DNA could adopt a state in which the NTDs were farther apart leading to low FRET. Indeed, constant temperature simulations revealed a similar broad distribution in distances between labeling positions with a major population with ~30 Å distance as in the crystal structure and another major population with a larger distance that would lead to lower FRET (Fig. 3D).

Relative domain motions on the seconds timescale. Besides the stable traces observed for free NFκB, 17% of the smFRET traces were classified as fluctuating (Fig. 2C, S28-32), based on the fluctuations between different states during the observation time. In some traces, the motions were large enough to connect low- and high-FRET states, corresponding to a 70 Å to 30 Å inter-dye distance change (Fig. 4A). The motions displayed a high level of heterogeneity and, as was the case for the long-lived states, could not be described by a few discrete states. In other traces (Fig. 4B), the two domains fluctuated around a low-FRET state (FRET efficiency ~0.25, distance ~60 Å), and then transitioned to a high-FRET state (FRET efficiency ~0.8, distance ~40 Å) and fluctuated around that value. We also observed that NFκB molecules transitioned from a fluctuating state to a long-lived state where they could be temporarily

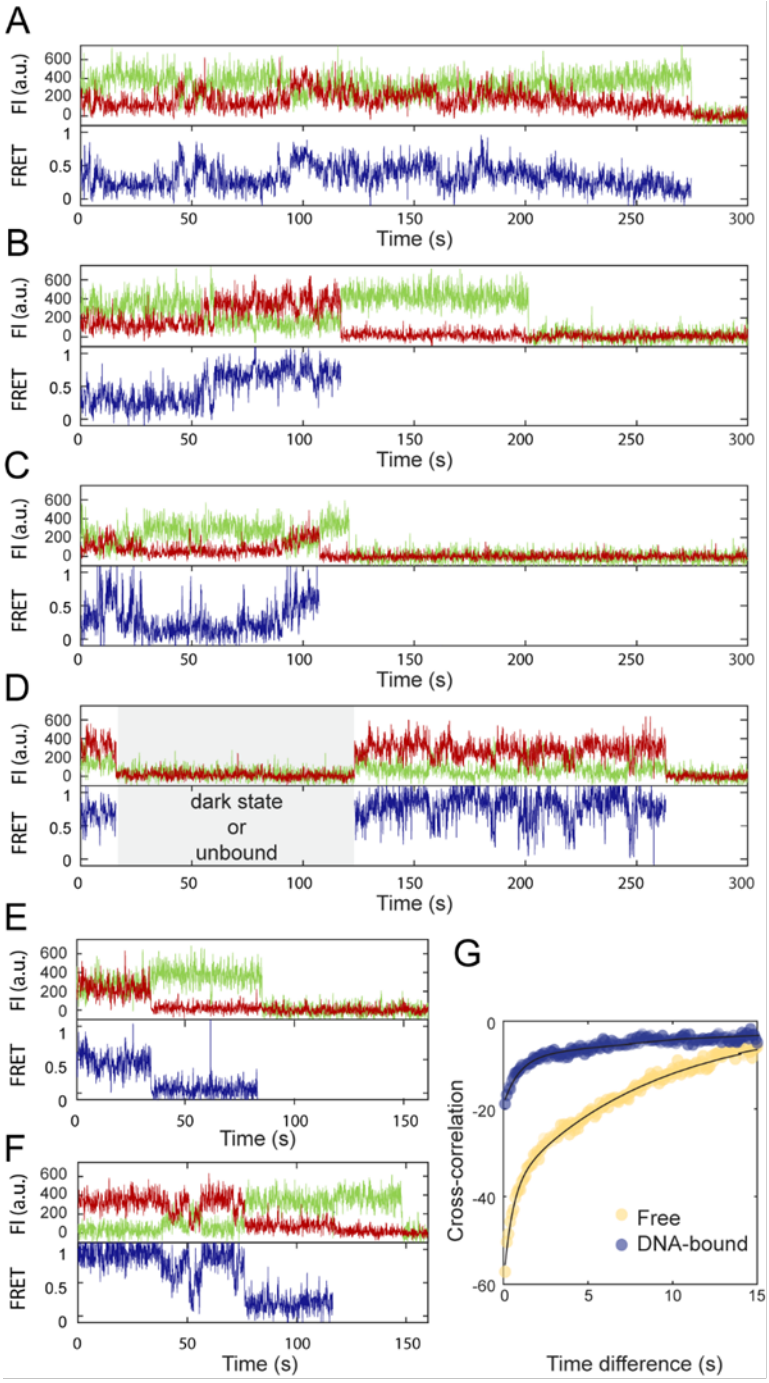

Fig. 4. Fluctuating smFRET traces of NFκB showing relative domain motions and the hierarchy of a rugged energy landscape. (A) Representative fluctuating traces for free NFκB with fluctuations connecting low- and high- FRET states, which corresponds 30 - 70 Å in inter-dye distance. (B) A trace for free NFκB with small fluctuations around a low-FRET state at first. At 60 seconds, the molecule transitioned to a high-FRET state and fluctuated around it. (C) A trace with transitions between fluctuations and long-lived states for free NFκB, suggesting all the conformational states are interconvertible. (D and E) Representative fluctuating traces of DNA-bound NFκB showing small fluctuations in DNA-bound NFκB. The time period with no signals (grey area) could be caused by a donor dark state, an unbound state, or a state in which an unlabeled NFκB is bound to the immobilized DNA. (F) A trace with transitions between fluctuating and long-lived states for DNA-bound NFκB. (G) Cross-correlation analyses for fluctuations of free (yellow) and DNA-bound (blue) NFκB showing that the relative domain motions of the DNA-bound NFκB have lower amplitudes and slower rates. Bi-exponential fitting revealed the characteristic fluctuation time to be 0.5 s and 8.4 s for free NFκB and 0.9 s and 17 s for DNA-bound NFκB. Dot: data; Line: fit.

trapped (Fig. 4C). This again confirmed the long-lived states are not static but are interconvertible with other shorter-lived conformational states. The fluctuations were subjected to cross-correlation analysis for the donor and acceptor signals. The cross-correlation monotonically decayed as a function of time, suggesting no periodicity for the relative domain motions, and reflecting the stochastic diffusion-like dynamics of single protein domains (Fig. 4G). The cross-correlation for fluctuations in free NFκB could be fitted with a bi-exponential function giving decay rates of 2.0 ± 0.3 s-1 and 0.12 ± 0.01 s-1 and amplitudes of 22 ± 2 and 38 ± 1 respectively. Characteristic fluctuation times, defined as the reciprocal of the rates, were 0.5 seconds and 8.4 seconds. We also examined the effect of ionic strength on the domain motions. A series of smFRET experiments with NaCl concentrations from 100 mM to 250 mM showed

that the percentage of fluctuating traces (Fig. S4A) and fluctuating time scale (Fig. S4B) are dependent on ionic strength but not with a simple monotonic trend.

Fluctuation Times for DNA-Bound NFκB. NFκB bound to immobilized DNA also showed fluctuations on the seconds timescale. However, large-scale fluctuations connecting low- and high-FRET states were no longer observed (Fig. 4D, E, S44-46). As in free NFκB, DNA-bound NFκB also transitioned between fluctuating states and long-lived states (Fig. 4F). Cross-correlation analysis of fluctuations in DNA-bound NFκB yielded decay rates of 1.1 ± 0.2 s-1 and 0.06 ± 0.01 s-1 and amplitudes of 11 ± 1 and 8.4 ± 0.6 respectively. The corresponding fluctuation times were 0.9 seconds and 17 seconds. The smaller amplitudes reflect the lack of fluctuations connecting low- and high-FRET states. Both times are two-fold slower than those for free NFκB. The decreased fluctuation amplitudes and rates for DNA-bound NFκB are expected from the additional electrostatic interactions introduced by the negatively charged

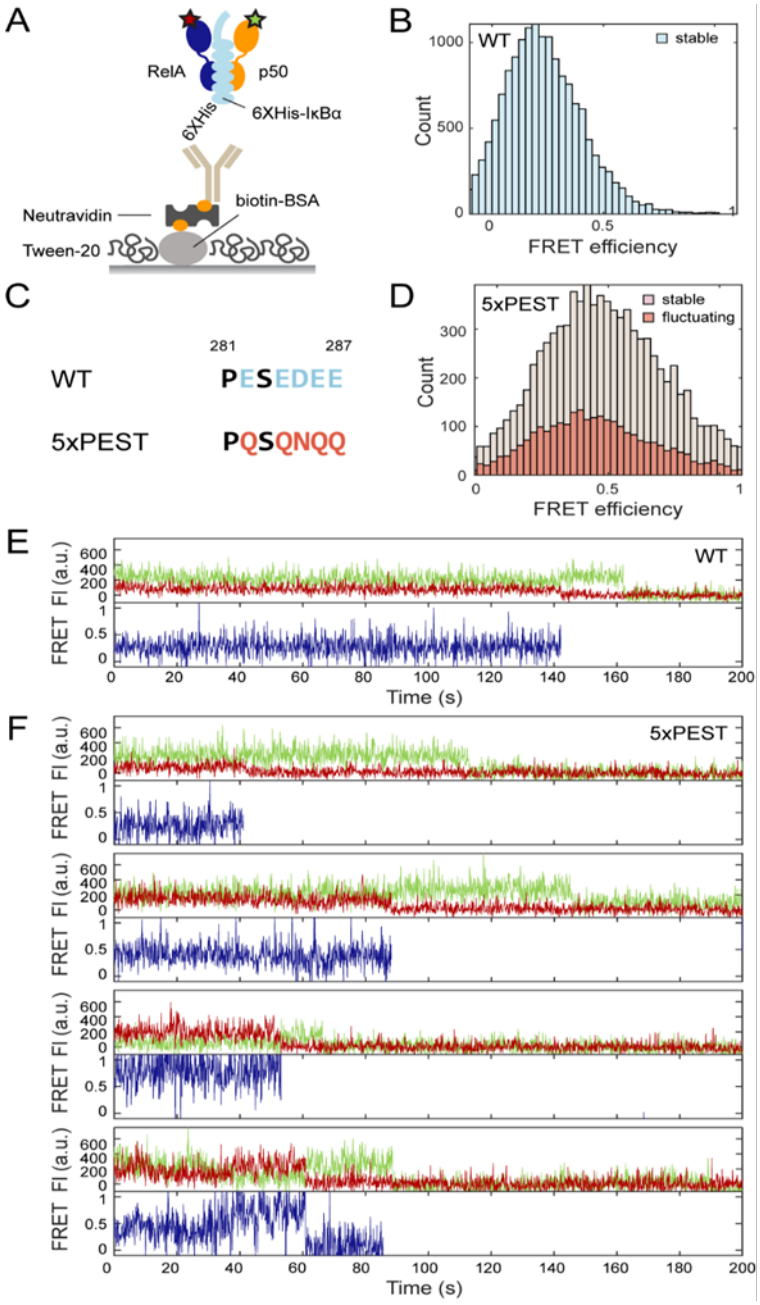

Fig. 5. smFRET experiments for IκBα-bound NFκB. (A) The experimental schematic. A His-tag on IκBα was used to immobilize the NFκB-IκBα complex through the interaction with anti-His antibody biotin conjugate. (B) FRET histogram showing the distribution of NFκB molecules bound to IκBα. Only a stable low FRET state was observed. (C) Five negatively charged residues in the wild type (WT) IκBα PEST sequence were mutated into neutral residues to generate the stripping impaired 5xPEST mutant. (D) FRET histogram for NFκB bound to the 5xPEST IκBα showing a broad distribution and a larger proportion of fluctuating traces. (E) A representative trace of NFκB bound to WT IκBα showing the stable low-FRET state. (F) Representative traces of NFκB bound to 5xPEST IκBα showing heterogeneous long-lived states with low- to mid- to high-FRET efficiencies and domain fluctuations. Other long-lived states with different FRET efficiencies are shown in SI.

DNA.

IκBα Locks the NFκB Domain Motions through the PEST sequence. To investigate how the inhibitor protein, IκBα, that strips NFκB from DNA and prevents DNA rebinding affects the relative domain motions of NFκB, we carried out smFRET experiments for IκBα-bound NFκB. For these experiments, non-tagged RelA-p50 dimer was used and IκBα was immobilized via a N-terminal His-tag (Fig. 5A). The FRET histogram constructed from 168 traces showed that every IκBα-bound NFκB populated a stable low-FRET state (Fig. 5B, E, S47-57). The histogram built by counting each visit to a long-lived state revealed a narrow conformational distribution in the range of 0.1 to 0.4 FRET efficiency (56 to 74 Å inter-dye distance) (Fig. S5A). All traces contained long-lived states with lifetime longer than the photobleaching lifetime. No anticorrelation of donor and acceptor signals were observed (Fig. S2C), suggesting the relative domain motions displayed in free and DNA-bound NFκB were completely suppressed by IκBα. Transitions between long-lived states were not observed either. The results show that IκBα reduced the conformational heterogeneity in NFκB and locked the domain motions to a stable low-FRET state.

We next performed the same experiment for NFκB bound to the 5xPEST IκBα mutant, which contains charge-neutralizing mutations E282Q/E284Q/D285N/E286Q/E287Q in the C-terminal disordered PEST sequence and is impaired in its molecular stripping function (Fig. 5C) [15]. The results showed that, in contrast to wildtype, 5xPEST IκBα was not able to lock the NFκB domain motions to a stable low-FRET state. Instead, 5xPEST IκBα-bound NFκB displayed a broad distribution of long-lived states and domain fluctuations as was observed in free NFκB (Fig. 5D, F, S58-64). Interestingly, we observed relatively more fluctuating traces in 5xPEST IκBα-bound NFκB, which implies that placing a charge-neutral polypeptide in between the NFκB NTDs may reduce the electrostatic interactions that lead to long-lived states. Our results show that the stripping and inhibitory function of IκBα is related to its ability to lock the NFκB NTDs in a fixed position, and that this function requires the negative charges on the IκBα PEST sequence.

Discussion

NFκB and suggest a hierarchical rugged energy landscape with many deep wells leading to long-lived conformational states interconvertible on the minutes timescale superimposed on a rough surface of substates that interconvert on the hundreds of milliseconds to seconds timescale. The large number of conformations constitute the continuous distribution and fluctuations observed by smFRET and cannot be described by just a few discrete states. A broad conformational distribution is a signature for intrinsically disordered proteins and denatured proteins [28], but has also been found in structured proteins [6,30,31]. Slow motions (>100 ms) on a rugged landscape have been reported for angstrom-scale fluctuations in a native enzyme [5] and nano-scale fluctuations in a denatured membrane protein [32]. However, this is the first time that a continuum of conformations connected by slow motions are directly resolved and visualized.

The slow motions of NFκB could originate from electrostatic interactions between domains. The non-uniform charge distribution in NFκB domains could drive relative motions between them as a result of balancing attractive and repulsive interactions. An analysis of the electrostatic potential of the NFκB RelA-p50 heterodimer revealed electrostatic repulsion between the NTDs as well as attraction between the NTD and the DD of p50, which could drive the large-scale conformational change to fully expose the DNA-binding cavity [10]. Electrostatic interactions between domains could also stabilize interfaces formed in their transient interactions, leading to the long-lived states observed in smFRET. The frustration between the many options for attractive and repulsive long-range electrostatic interactions among the protein domains could lead to slow large-scale motions. Indeed, varying the ionic strength altered the interdomain motions, and addition of the negatively charged DNA caused the motions to be even slower and

of reduced amplitude. The comparison between wild type and 5xPEST IκBα with a charge-neutral PEST also suggest that elimination of the conformational heterogeneity and dynamics is achieved through the highly negatively charged PEST sequence. Placing a charge-neutral polypeptide in between the NFκB NTDs reduces the electrostatic interactions that could lead to heterogeneous long-lived states, consistent with our hypothesis that the slow heterogeneous dynamics originated from electrostatic frustration.

Besides electrostatic interactions between domains, the linkers might also cause the interdomain motions to be slow. The highly conserved linker, with the sequence DNRAPNTAEL for RelA and DSKAPNASNL for p50, contains a proline and several charged residues, both of whichare known to increase the rigidity of disordered linkers [33]. In addition, prolines can undergo cis-trans isomerization on seconds to minutes timescale [34] and therefore could also contribute to the slow motions.

A rugged energy landscape can be very useful in signaling and regulation, processes in which efficiency and reversibility of macromolecular interactions are important. In the case of NFκB, the heterogenous long-lived states interconverting on the minutes time scale and the faster domain fluctuations on the seconds timescale could both be useful in controlling DNA association. We first compare the timescales of NF-κB motions with DNA binding rates. The average time needed for a DNA binding event can be estimated from the known rate constant (kon) 2.7×108 M-1s-1 [10] and the estimated nuclear concentration of κB sites (1-100 nM). By calculating 1/([κB sites]×kon) we obtain 0.1 – 10 seconds for a binding event. Recent in vivo single-molecule imaging showed the binding time of RelA to DNA to be in this same range [35]. The observed long-lived states typically have lifetimes longer a minute and thus can be considered static from the viewpoint of DNA binding. These long-lived states consist of a broad distribution of the positioning of the NTDs with respect to each other, each with a different degree of DNA-binding cavity exposure. It is likely that only some of them are the “open conformations” accessible for DNA binding. Such partitioning of the long-lived states could control the proportion of molecules accessible to DNA. Indeed, recent single-particle tracking experiments revealed a power-law dwell-time distribution for transcription factors binding to DNA, indicating a continuum of states with different binding affinities, consistent with our finding that NFκB exists in a continuum of long-lived conformational states with different degrees of DNA accessibility [36]. Furthermore, the domain motions characterized by fluctuation times 0.5 and 8.4 seconds are on the same timescale as the DNA-binding events. While the minutes motions may be used as a static control, the seconds motions are most likely coupled to DNA binding and could be a dynamic control in which the re-orientation of NTDs during the binding process, from first encountering DNA to forming a bound complex, affects the DNA-association kinetics.

On the other hand, the interdomain motions in DNA-bound NFκB can be useful for DNA dissociation by molecular stripping. Although the observation of a continuum of conformations seems to contradict the NFκB-DNA crystal structure, we speculate that the single structure is a result of overstabilization in the crystal. Similar findings of large-scale interdomain motions have been reported for the 627-NLS domain of the influenza polymerase by NMR, SAXS, and smFRET despite the existence of crystal structures [30]. Transcription factor binding to DNA and dissociation from DNA are the two time points defining the transcription time window, which controls the amount of mRNA produced [37]. In the NFκB-DNA-IκBα signaling network, we have previously shown that cessation of transcription occurs by IκBα-induced dissociation of NFκB from DNA [20], or molecular stripping [18]. Molecular stripping starts when IκBα encounters NFκB bound to DNA and involves formation of a transient IκBα-NFκB-DNA ternary complex [14]. Coarse-grained MD simulations predicted the observation herein that IκBα induces a twist in the NTDs so that only one NTD can make contacts with the DNA, lowering the barrier for DNA dissociation (15). Finally, DNA dissociates and is unable to rebind the remaining NFκB-IκBα complex [15]. With molecular stripping, the DNA dissociation rate is proportional to and thus

controlled by the IκBα concentration [14]. Just as the broad distribution of motional timescales in free NFκB can be useful to control DNA binding, those in NFκB-DNA may control the binding of IκBα to initiate molecular stripping. With smFRET, we observed that IκBα locked the NFκB NTDs in a static low-FRET state consistent with twisting and spreading away from a DNA-binding competent state. The fact that the stripping impaired 5xPEST IκBα still allowed conformational dynamics in DNA-bound NFκB strongly suggests that reorientating the NTDs to a static state is required for molecular stripping. The fact that the IκBα-bound NFκB is the only static state we observed also strongly suggests that NTD motions are required for DNA binding. Our results suggest that both functions of IκBα, molecular stripping and preventing DNA binding, come from altering the NFκB NTD motions. By reorienting the NTDs, IκBα lowers the DNA dissociation barrier, and by eliminating the conformational heterogeneity, IκBα inhibits NFκB-DNA interactions.

In conclusion, the extremely slow and heterogenous NFκB NTD motions observed by smFRET reveal a rugged energy landscape that can be reshaped by DNA and IκBα. NFκB adopts a continuous distribution of conformations that were completely unexpected based on previously reported crystal structures. We propose that the observed domain motions control the association and dissociation of NFκB and DNA to achieve efficient transcription activation and allow IκBα to efficiently terminate transcription.

Acknowledgments
The authors thank Hajin Kim at Ulsan National Institute of Science and Technology for his advice on setting up the TIRF microscope, Majid Ghassemian at the Biomolecular and Proteomics Mass Spectrometry Facility, UCSD for carrying out the mass spectrometry analyses, and Andy McCammon for helpful discussions. W.C. acknowledges fellowship support from the Taiwanese Ministry of Education.

Competing Interest Statement
The authors declare no competing interests

References

1 Smock, R. G. & Gierasch, L. M. Sending signals dynamically. *Science* **324**, 198-203, (2009).
2 Bryngelson, J. D., Onuchic, J. N., Socci, N. D. & Wolynes, P. G. Funnels, pathways, and the energy landscape of protein folding: a synthesis. *Proteins* **21**, 167-195, (1995).
3 Austin, R. H., Beeson, K. W., Eisenstein, L., Frauenfelder, H. & Gunsalus, I. C. Dynamics of ligand binding to myoglobin. *Biochemistry* **14**, 5355-5373, (1975).
4 Frauenfelder, H., Sligar, S. G. & Wolynes, P. G. The energy landscapes and motions of proteins. *Science* **254**, 1598-1603, (1991).
5 Yang, H. *et al.* Protein conformational dynamics probed by single-molecule electron transfer. *Science* **302**, 262-266, (2003).
6 Grossman-Haham, I., Rosenblum, G., Namani, T. & Hofmann, H. Slow domain reconfiguration causes power-law kinetics in a two-state enzyme. *Proc Natl Acad Sci U S A* **115**, 513-518, (2018).
7 Hu, X. H. *et al.* The dynamics of single protein molecules is non-equilibrium and self-similar over thirteen decades in time. *Nat Phys* **12**, 171-174, (2016).

8 Amoutzias, G. D., Robertson, D. L., Van de Peer, Y. & Oliver, S. G. Choose your partners: dimerization in eukaryotic transcription factors. *Trends Biochem Sci* **33**, 220-229, (2008).
9 Vuzman, D., Polonsky, M. & Levy, Y. Facilitated DNA search by multidomain transcription factors: cross talk via a flexible linker. *Biophys J* **99**, 1202-1211, (2010).
10 Narang, D., Chen, W., Ricci, C. G. & Komives, E. A. RelA-Containing NFkappaB Dimers Have Strikingly Different DNA-Binding Cavities in the Absence of DNA. *J Mol Biol* **430**, 1510-1520, (2018).
11 Traenckner, E. B. & Baeuerle, P. A. Appearance of apparently ubiquitin-conjugated I kappa B-alpha during its phosphorylation-induced degradation in intact cells. *J Cell Sci Suppl* **19**, 79-84, (1995).
12 Hoffmann, A., Levchenko, A., Scott, M. L. & Baltimore, D. The IkappaB-NF-kappaB signaling module: temporal control and selective gene activation. *Science* **298**, 1241-1245, (2002).
13 Arenzana-Seisdedos, F. *et al.* Nuclear localization of I kappa B alpha promotes active transport of NF-kappa B from the nucleus to the cytoplasm. *Journal of cell science* **110**, 369-378, (1997).
14 Alverdi, V., Hetrick, B., Joseph, S. & Komives, E. A. Direct observation of a transient ternary complex during IkappaBalpha-mediated dissociation of NF-kappaB from DNA. *Proc Natl Acad Sci U S A* **111**, 225-230, (2014).
15 Dembinski, H. E. *et al.* Functional importance of stripping in NFkappaB signaling revealed by a stripping-impaired IkappaBalpha mutant. *Proc Natl Acad Sci U S A* **114**, 1916-1921, (2017).
16 Huxford, T., Huang, D.-b., Malek, S. & Ghosh, G. The crystal structure of the IκBα/NF-κB complex reveals mechanisms of NF-κB inactivation. *Cell* **95**, 759-770, (1998).
17 Jacobs, M. D. & Harrison, S. C. Structure of an IκBα/NF-κB complex. *Cell* **95**, 749-758, (1998).
18 Potoyan, D. A., Zheng, W., Komives, E. A. & Wolynes, P. G. Molecular stripping in the NF-kappaB/IkappaB/DNA genetic regulatory network. *Proc Natl Acad Sci U S A* **113**, 110-115, (2016).
19 Potoyan, D. A., Zheng, W., Ferreiro, D. U., Wolynes, P. G. & Komives, E. A. PEST Control of Molecular Stripping of NFkappaB from DNA Transcription Sites. *J Phys Chem B* **120**, 8532-8538, (2016).
20 Bergqvist, S. *et al.* Kinetic enhancement of NF-kappaBxDNA dissociation by IkappaBalpha. *Proc Natl Acad Sci U S A* **106**, 19328-19333, (2009).
21 Croy, C. H., Bergqvist, S., Huxford, T., Ghosh, G. & Komives, E. A. Biophysical characterization of the free IkappaBalpha ankyrin repeat domain in solution. *Protein Sci* **13**, 1767-1777, (2004).
22 Hua, B. *et al.* An improved surface passivation method for single-molecule studies. *Nat Methods* **11**, 1233-1236, (2014).
23 Lamboy, J. A., Kim, H., Dembinski, H., Ha, T. & Komives, E. A. Single-molecule FRET reveals the native-state dynamics of the IkappaBalpha ankyrin repeat domain. *J Mol Biol* **425**, 2578-2590, (2013).
24 Lu, W. *et al.* OpenAWSEM with Open3SPN2: A fast, flexible, and accessible framework for large-scale coarse-grained biomolecular simulations. *PLoS Comput Biol* **17**, e1008308, (2021).
25 Chin, J. W. *et al.* Addition of p-azido-L-phenylalanine to the genetic code of Escherichia coli. *J Am Chem Soc* **124**, 9026-9027, (2002).
26 Jewett, J. C. & Bertozzi, C. R. Cu-free click cycloaddition reactions in chemical biology. *Chem Soc Rev* **39**, 1272-1279, (2010).

27 Berkowitz, B., Huang, D. B., Chen-Park, F. E., Sigler, P. B. & Ghosh, G. The x-ray crystal structure of the NF-kappa B p50.p65 heterodimer bound to the interferon beta -kappa B site. *J Biol Chem* **277**, 24694-24700, (2002).
28 Hellenkamp, B. *et al.* Precision and accuracy of single-molecule FRET measurements-a multi-laboratory benchmark study. *Nat Methods* **15**, 669-676, (2018).
29 Huang, D. B. *et al.* Crystal structure of NF-kappaB (p50)2 complexed to a high-affinity RNA aptamer. *Proc Natl Acad Sci U S A* **100**, 9268-9273, (2003).
30 Delaforge, E. *et al.* Investigating the Role of Large-Scale Domain Dynamics in Protein-Protein Interactions. *Front Mol Biosci* **3**, 54, (2016).
31 Huang, J. R. *et al.* Transient electrostatic interactions dominate the conformational equilibrium sampled by multidomain splicing factor U2AF65: a combined NMR and SAXS study. *J Am Chem Soc* **136**, 7068-7076, (2014).
32 Krainer, G. *et al.* Slow Interconversion in a Heterogeneous Unfolded-State Ensemble of Outer-Membrane Phospholipase A. *Biophys J* **113**, 1280-1289, (2017).
33 Sorensen, C. S. & Kjaergaard, M. Effective concentrations enforced by intrinsically disordered linkers are governed by polymer physics. *Proc Natl Acad Sci U S A* **116**, 23124-23131, (2019).
34 Brandts, J. F., Halvorson, H. R. & Brennan, M. Consideration of the Possibility that the slow step in protein denaturation reactions is due to cis-trans isomerism of proline residues. *Biochemistry* **14**, 4953-4963, (1975).
35 Callegari, A. *et al.* Single-molecule dynamics and genome-wide transcriptomics reveal that NF-kB (p65)-DNA binding times can be decoupled from transcriptional activation. *PLoS Genet* **15**, e1007891, (2019).
36 Garcia, D. A. *et al.* Power-law behavior of transcription factor dynamics at the single-molecule level implies a continuum affinity model. *Nucleic Acids Res*, (2021).
37 Lammers, N. C. *et al.* Multimodal transcriptional control of pattern formation in embryonic development. *Proc Natl Acad Sci U S A* **117**, 836-847, (2020).